

# Glycogen phosphorylase revisited: extending the resolution of the R- and T-state structures of the free enzyme and in complex with allosteric activators

Demetres D. Leonidas,<sup>a\*</sup> Spyros E. Zographos,<sup>b\*</sup> Katerina E. Tsitsanou,<sup>b</sup> Vassiliki T. Skamnaki,<sup>a</sup> George Stravodimos<sup>a</sup> and Efthimios Kyriakis<sup>a</sup>

Received 9 June 2021

Accepted 16 August 2021

Edited by R. Sankaranarayanan, Centre for Cellular and Molecular Biology, Hyderabad, India

This publication is dedicated to the memory of Professor L. N. Johnson and Dr N. G. Oikonomakos, who were the pioneers in crystallographic studies of glycogen phosphorylase.

**Keywords:** glycogen phosphorylase; glycogen metabolism; allosteric transitions.

**PDB references:** rabbit muscle glycogen phosphorylase, R-state, 3e3l; T-state, 7p7d; complex with AMP, R-state, 3e3n; complex with IMP, R-state, 3e3o

**Supporting information:** this article has supporting information at journals.iucr.org/f

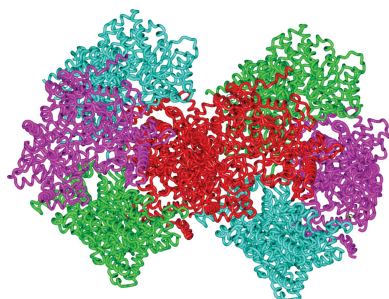
<sup>a</sup>Department of Biochemistry and Biotechnology, University of Thessaly, Biopolis, 41500 Larissa, Greece, and

<sup>b</sup>Institute of Chemical Biology, National Hellenic Research Foundation, Vassileos Constantinou Avenue, 11635 Athens, Greece. \*Correspondence e-mail: ddleonidas@bio.uth.gr, sez@eie.gr

The crystal structures of free T-state and R-state glycogen phosphorylase (GP) and of R-state GP in complex with the allosteric activators IMP and AMP are reported at improved resolution. GP is a validated pharmaceutical target for the development of antihyperglycaemic agents, and the reported structures may have a significant impact on structure-based drug-design efforts. Comparisons with previously reported structures at lower resolution reveal the detailed conformation of important structural features in the allosteric transition of GP from the T-state to the R-state. The conformation of the N-terminal segment (residues 7–17), the position of which was not located in previous T-state structures, was revealed to form an  $\alpha$ -helix (now termed  $\alpha 0$ ). The conformation of this segment (which contains Ser14, phosphorylation of which leads to the activation of GP) is significantly different between the T-state and the R-state, pointing in opposite directions. In the T-state it is packed between helices  $\alpha 4$  and  $\alpha 16$  (residues 104–115 and 497–508, respectively), while in the R-state it is packed against helix  $\alpha 1$  (residues 22'–38') and towards the loop connecting helices  $\alpha 4'$  and  $\alpha 5'$  of the neighbouring subunit. The allosteric binding site where AMP and IMP bind is formed by the ordering of a loop (residues 313–326) which is disordered in the free structure, and adopts a conformation dictated mainly by the type of nucleotide that binds at this site.

## 1. Introduction

Glycogen phosphorylase (GP; EC 2.4.1.1) is a key enzyme in glycogen metabolism that catalyzes the first step in the degradation of glycogen to yield glucose 1-phosphate (glucose-1-P; Oikonomakos, 2002). As such, GP has a pivotal role in human carbohydrate catabolism by initiating the enzyme cascade that releases glucose from glycogen deposits to serve the energy needs of the organism (Agius, 2015). Because of the central role of GP in glucose homeostasis, the enzyme has been investigated for therapeutic intervention in type 2 diabetes and validated as a molecular target for the discovery of novel antidiabetic drugs that will inhibit hepatic glucose production (Treadway *et al.*, 2001). X-ray crystallographic studies and kinetic experiments have led to the identification of seven ligand-binding sites in GP. These include the active site (where the breakdown of glycogen occurs), the inhibitor site (where purine-based inhibitors, such as caffeine, bind and obstruct the entrance to the active site), the allosteric site (where the binding of ligands activates the enzyme), the new allosteric site or drug site (located at the interface in the biological dimer), the storage site (where glycogen and oligosaccharides bind; Oikonomakos, 2002) and more recently two new sites where binding elicits allosteric



activation of GPb: the benzimidazole site (Chrysin *et al.*, 2005) and the quercetin site (Kantsadi *et al.*, 2014).

Glycogen phosphorylase was the first allosteric enzyme to be discovered (Johnson & Barford, 1990). It was isolated and characterized by Carl F. Cori, Gerhard Schmidt and Gerty T. Cori (Cori *et al.*, 1939; Cori & Cori, 1940). Arda Green and Gerty Cori crystallized it for the first time in 1943 (Green & Cori, 1943) and illustrated that glycogen phosphorylase exists in two interconvertible forms, *b* and *a*, depending on its phosphorylation state, as well as in the R-state or T-state based on the presence of AMP (Cori & Green, 1943). Phosphorylase *b* (GPb) is inactive but can be allosterically activated by AMP or IMP and by the phosphorylation of one specific serine residue (Ser14) by phosphorylase kinase, producing the active phosphorylase *a* (GPa), while the reverse dephosphorylation reaction and deactivation of the enzyme is catalyzed by phosphatase 1 (Johnson, 1992). The activation of the enzyme by AMP or phosphorylation can be understood as a conversion from the dimeric T-state (low affinity) to the dimeric R-state (high affinity) according to the Monod, Wyman and Changeux model (Monod *et al.*, 1965). High concentrations of substrate anions and of anions high in the Hofmeister series such as sulfate are also able to activate phosphorylase *b* to a considerable extent (Barford & Johnson, 1989; Lorek *et al.*, 1984) and this activation can be further stimulated by AMP (Leonidas *et al.*, 1991). Analysis of the R-state rabbit muscle GPb (rmGPb) crystal structure in the presence of sulfate anions (Barford & Johnson, 1989) revealed that sulfate mimics the substrate phosphate by binding to the serine phosphate site, resulting in localized changes in tertiary structure. These changes are coupled to large changes in quaternary structure which directly affect the AMP and the Ser14 phosphate site and indirectly affect the catalytic site (Barford & Johnson, 1989). The ammonium sulfate activation of rmGPb has been confirmed by kinetic studies (Leonidas *et al.*, 1990, 1991) and it was concluded that the sulfate groups take the place of the phosphate at the GP phosphorylation site at Ser14. *In vitro* activation of the enzyme is accompanied by a dimer-to-tetramer conversion (Leonidas *et al.*, 1991).

The allosteric site is formed by residues from the two symmetrically related subunits of the functional GP dimer, located on opposite sides of the enzyme molecule. Two  $\alpha$ -helices (residues 47–78 and 289–314) and four  $\beta$ -strands (residues 153–160, 191–193, 222–232 and 237–247) create a V-shaped cavity which is closed by the cap' region (residues 36'–47' from the symmetry subunit) to form the allosteric site (Oikonomakos, 2002). The allosteric site recognizes a variety of phosphorylated compounds such as AMP, IMP, ATP, glucose 6-phosphate, NADH, UDP-glucose, 2-deoxyglucose 6-phosphate,  $\beta$ -glycerophosphate and inorganic phosphate. The most potent ligand binding at this site is AMP, with  $K_a$  values for GPb and GPa of 63 and 0.3  $\mu$ M, respectively (Leonidas *et al.*, 1990). The binding of ligands at this site inhibits GP activity either by competing with the physiological activator AMP or by stabilizing the inactive T-state conformation of the enzyme (Oikonomakos, 2002; Somsák *et al.*, 2008; Hayes *et al.*, 2014; Stravodimos *et al.*, 2017).

There are three glycogen phosphorylase isoforms in the liver, muscle and brain. Crystal structures of human muscle GPa (Lukacs *et al.*, 2006), the human liver enzyme (hIGP; Rath *et al.*, 2000) and the human brain enzyme (Mathieu *et al.*, 2016) have been reported. Although the pharmacologically relevant target is hIGP, most crystallographic studies of GP are performed with rmGPb due to the ease of growing crystals that are suitable for inhibitor studies. Thus, the very first GP structures reported were of the dimeric T-state rmGPb (Acharya *et al.*, 1991) and rmGPa (Sprang & Fletterick, 1979), followed by the tetrameric R-state rmGPb (Barford & Johnson, 1989) and rmGPa (Barford *et al.*, 1991) structures. RmGP and hIGP share 97% sequence homology and both enzymes are fully conserved in sequence and structure at the active site; thus, any structural analysis of rmGPb is applicable to hIGP. This has been demonstrated in several inhibitor studies (Kantsadi *et al.*, 2016, 2017; Bokor *et al.*, 2017; Kun *et al.*, 2018; Kyriakis *et al.*, 2018, 2020; Chetter *et al.*, 2020; Fischer *et al.*, 2019). In the last 30 years many inhibitor studies have been reported which have led to the discovery of potent and specific GP inhibitors (Oikonomakos, 2002; Oikonomakos & Somsák, 2008; Somsák *et al.*, 2008; Somsák, 2011; Stravodimos *et al.*, 2017; Hayes *et al.*, 2014).

The crystal structures of free rmGPb in the T-state and the R-state or in the form activated by AMP used in comparative structural analysis of the binding of the inhibitors and subsequent structure-driven inhibitor-design studies were at rather low resolution [T-state rmGPb, 1.9 Å, PDB entry 1gpb (Acharya *et al.*, 1991); R-state rmGPb, 2.9 Å, PDB entry 9gpb (Barford & Johnson, 1989); R-state rmGPb–AMP, 2.9 Å, PDB entry 7gpb (Barford *et al.*, 1991)] and were determined using X-ray diffraction data collected from preformed crystals diffused with AMP. High-resolution data are essential in the analysis of protein–inhibitor interactions to assist in structure-guided inhibitor-development studies. Thus, we now report structures of T-state and R-state free rmGPb together with those of R-state rmGPb in complex with AMP and IMP at high resolution using X-ray data collected from crystals grown from preformed rmGPb–AMP and rmGPb–IMP complexes.

## 2. Materials and methods

### 2.1. Crystallization and data collection

RmGPb was purified following previously established protocols (Drakou *et al.*, 2020), while T-state rmGPb crystals were grown by the batch method as described previously (Fischer *et al.*, 2019). Free R-state rmGPb crystals were grown from 1.2–1.4 M ammonium sulfate, 10 mM  $\beta$ -glycerophosphate buffer pH 7.5, 0.5 mM EDTA using the microdialysis method as described previously (Leonidas, Oikonomakos, Papageorgiou, Acharya *et al.*, 1992). Crystals of the R-state rmGPb–AMP and rmGPb–IMP complexes were grown using the same conditions as used for the free enzyme, with the exception that the enzyme solution was supplemented with 2 mM AMP or 6 mM IMP prior to crystallization. Under these crystallization conditions rmGPb exists as a tetramer and is

Table 1

Data-processing and refinement statistics.

Values in parentheses are for the outermost shell.

|                                      | rmGPb (R-state)       | rmGPb-AMP (R-state)                     | rmGPb-IMP (R-state)   | rmGPb (T-state)        |
|--------------------------------------|-----------------------|---|-----------------------|------------------------|
| PDB entry                            | 3e3l                  | 3e3n                                    | 3e3o                  | 7p7d                   |
| Space group                          | $P2_1$                | $P2_1$                                  | $P2_1$                | $P4_32_12$             |
| $a, b, c$ (Å)                        | 118.89, 189.92, 88.16 | 119.02, 188.08, 175.91                  | 118.68, 188.45, 87.85 | 126.28, 126.28, 115.36 |
| $\alpha, \beta, \gamma$ (°)          | 90, 109.27, 90        | 90, 109.82, 90                          | 90, 109.10, 90        | 90, 90, 90             |
| Resolution (Å)                       | 30.0–2.6 (2.70–2.60)  | 30.0–2.7 (2.74–2.70)                    | 30.0–2.6 (2.66–2.60)  | 115.4–1.45 (1.47–1.45) |
| No. of observations                  | 626958                | 1244255                                 | 424414                | 1196324                |
| No. of unique reflections            | 107281                | 189160                                  | 105631                | 164062                 |
| $R_{\text{meas}}$                    | 0.06 (0.37)           | 0.07 (0.47)                             | 0.05 (0.50)           | 0.08 (0.66)            |
| Completeness (%)                     | 99.6 (99.6)           | 94.1 (89.8)                             | 99.5 (96.4)           | 100 (99.9)             |
| $\langle I/\sigma(I) \rangle$        | 11.7 (3.9)            | 6.2 (1.7)                               | 14.7 (2.8)            | 13.6 (3.0)             |
| $CC_{1/2}$                           | 0.997 (0.930)         | 0.995 (0.545)                           | 0.996 (0.832)         | 0.996 (0.940)          |
| Wilson $B$ factor (Å <sup>2</sup> )  | 60.9                  | 50.2                                    | 65.1                  | 19.1                   |
| $R_{\text{cryst}}$                   | 0.207 (0.309)         | 0.192 (0.288)                           | 0.201 (0.270)         | 0.130 (0.228)          |
| $R_{\text{free}}$                    | 0.266 (0.374)         | 0.258 (0.349)                           | 0.267 (0.346)         | 0.170 (0.245)          |
| No. of protein atoms                 | 26267                 | 52714                                   | 26286                 | 6664                   |
| No. of ligand atoms                  | —                     | 184                                     | 92                    | —                      |
| No of sulfate molecules              | 12                    | 16                                      | 8                     | —                      |
| No. of water molecules               | 110                   | 350                                     | 116                   | 794                    |
| R.m.s.d., bond lengths (Å)           | 0.010                 | 0.009                                   | 0.011                 | 0.011                  |
| R.m.s.d., angles (°)                 | 1.3                   | 1.2                                     | 1.4                   | 1.6                    |
| Ramachandran statistics              |                       |   |                       |                        |
| Favoured (%)                         | 92                    | 94                                      | 93                    | 97                     |
| Allowed (%)                          | 6                     | 5                                       | 6                     | 3                      |
| Outliers (%)                         | 2                     | 1                                       | 1                     | 0                      |
| Average $B$ factor (Å <sup>2</sup> ) |                       |   |                       |                        |
| Protein atoms                        | 49.8                  | 41.0                                    | 43.9                  | 26.4                   |
| Water molecules                      | 50.7                  | 28.8                                    | 55.1                  | 39.1                   |
| Ligand atoms (A/B/C/D/E/F/G/H)       | —                     | 28.3/35.1/33.0/30.6/37.8/26.3/29.1/34.3 | 79.7/55.6/53.0/67.8   | —                      |
| Sulfate atoms                        | 56.3                  | 46.5                                    | 93.7                  | —                      |

practically saturated by AMP or IMP (Leonidas, Oikonomakos, Papageorgiou & Sotiroudis, 1992). All R-state crystals belonged to the monoclinic space group  $P2_1$ , and the free rmGPb and rmGPb-IMP crystals have very similar unit-cell dimensions (Table 1). In contrast, the rmGPb-AMP complex crystals have unit-cell dimensions  $a = 119$ ,  $b = 190$ ,  $c = 176$  Å,  $\beta = 110^\circ$ . In this crystal form the  $c$  dimension is twice the  $c$  dimension of the crystal form of the free R-state. This results in a doubling of the unit-cell volume, and as a consequence there are two tetramers per asymmetric unit instead of one.

Crystallographic data for free R-state rmGPb to 2.6 Å resolution and for the R-state rmGPb-AMP complex to 2.7 Å resolution were collected on an ADSC Quantum 4 CCD detector using synchrotron radiation at stations PX10.1 ( $\lambda = 0.97976$  Å) and PX9.6 ( $\lambda = 0.87$  Å) of the Synchrotron Radiation Source, CCLRC, Daresbury Laboratory, UK, respectively. X-ray diffraction data for the T-state rmGPb structure to 1.45 Å resolution and for the R-state rmGPb-IMP complex to 2.6 Å resolution were collected at station P13 ( $\lambda = 0.9763$  Å) of the EMBL Hamburg Outstation on a PILATUS detector and at station X13 ( $\lambda = 0.8063$  Å) on a MAR Research CCD detector, respectively. All data sets were collected using one crystal of each protein at room temperature, except for the T-state rmGPb, where data were collected (from one crystal) at 100 K [growth medium supplemented with 30% (v/v) DMSO was used as a cryoprotectant]. For the room-temperature data sets each crystal was translated four times to avoid any radiation damage. For all R-state rmGPb data sets, crystal orientation, integration of reflections, inter-

frame scaling, partial reflection summation, data reduction and post-refinement were all performed using the *HKL* suite of programs (Otwinowski & Minor, 1997). X-ray diffraction data from the T-state rmGPb crystal were processed using the *XDS* program (Kabsch, 2010), scaled by *AIMLESS* (Evans & Murshudov, 2013) and transformed to amplitudes using *CTRUNCATE* (French & Wilson, 1978) from the *CCP4* suite of programs (Winn *et al.*, 2011).

## 2.2. Structure determination and refinement

The free T-state and R-state rmGPb structures were determined using previously determined structures (PDB entries 1gpb and 9gpb, respectively) as the starting models for initial phase determination. For the rmGPb-IMP structure the free structure presented here was used as the starting model for further refinement. For the R-state rmGPb-AMP complex data the real-space self-rotation function with origin removal, as implemented in *CNS* (Brünger *et al.*, 1998), showed a single strong peak at  $\kappa = 180^\circ$ , indicating twofold noncrystallographic symmetry. Assuming two rmGPb tetramers per crystallographic asymmetric unit, the Matthews coefficient (Matthews, 1968) is  $2.4 \text{ Å}^3 \text{ Da}^{-1}$ , while approximately 48% of the crystal volume is occupied by solvent. The complex structure was solved using the molecular-replacement method in *Phaser* (Storoni *et al.*, 2004) with the tetrameric R-state crystal structure of rmGPb (PDB entry 9gpb; Barford & Johnson, 1989) as the model. Using reflections in the resolution range 30.0–4.2 Å and no  $\sigma$  cutoff, two unique subunits were identified

by *Phaser*. Alternate cycles of manual building with *Coot* (Emsley *et al.*, 2010) and refinement using the maximum-likelihood target function as implemented in *REFMAC* (Murshudov *et al.*, 2011) improved the model. AMP and sulfate anions were included during the final stages of refinement. All data were included in the refinement procedure with no  $\sigma$  cutoff, and noncrystallographic symmetry (NCS) restraints were initially imposed. The NCS restraints were gradually relaxed during the course of the refinement and were removed in the final cycle. In the final round, TLS (translation–libration–screw) refinement within *REFMAC* was performed using TLS protein segments generated by the *TLSMD* web server (Painter & Merritt, 2006), which considerably improved the final model. *PROCHECK* (Laskowski *et al.*, 1993) was used to assess the quality of the final structure. Analysis of the Ramachandran ( $\varphi$ – $\psi$ ) plot showed that all residues lie in allowed regions. Solvent-accessible areas were calculated using *PISA* (Krissinel & Henrick, 2007). Details of the data-processing and refinement statistics are provided in Table 1. The rmGP structures were superimposed over well defined residues using *LSQKAB* (Winn *et al.*, 2011). Coordinates for all structures have been deposited in the RCSB Protein Data Bank (<http://www.rcsb.org/>) with the PDB codes reported in Table 1. All figures were prepared with *CCP4mg* (McNicholas *et al.*, 2011).

### 3. Results and discussion

#### 3.1. Overall structure

The asymmetric unit of the rmGPb–AMP complex from co-crystallization contains two tetramers, subunits *A*, *B*, *C* and *D* and the structurally equivalent subunits *E*, *F*, *G* and *H*, which are related by translational NCS along the *c* axis (an almost exact *c*/2 translation) and an almost 180° rotation around the axis of the molecular 222 symmetry of the tetramer (Fig. 1). The association of individual R-state subunits to form the dimer results in the burial of 3995 Å<sup>2</sup> of solvent-accessible area (33%) per subunit. The corresponding burial of solvent-accessible area on the association of the dimers to form the tetramer is 5085 Å<sup>2</sup> (47%) per subunit. The change in solvent-accessible area on association of the two tetramers is 5344 Å<sup>2</sup> (49%) per subunit, while the total buried surface area is 42 760 Å<sup>2</sup>. The tetrameric association has been described extensively previously (Barford & Johnson, 1989, 1992). The two rmGPb tetramers in the asymmetric unit are almost identical to the tetramer found in the previously reported rmGPb–AMP complex structure (PDB entry 7gpb; Barford *et al.*, 1991). The r.m.s.d. values for all atoms between the rmGPb–AMP tetramer (PDB entry 7gpb) and each of the two tetramers in the asymmetric unit of the rmGPb–AMP complex over the well defined residues 10–282 and 287–837 are 1.0 and 1.1 Å, respectively. The association of the two tetramers is supported by four direct hydrogen bonds and 11 van der Waals interactions between equivalent subunits *D* and *H* of the two tetramers (Table 2), while the calculated change in solvent free energy is  $-359 \text{ kcal mol}^{-1}$ . *PISA* buried-surface analysis

**Table 2**

Interactions between the two rmGPb tetramers in the rmGPb–AMP complex.

| Atom                       | Subunit  | Atom                   | Subunit  | Distance (Å) |
|----------------------------|----------|------------------------|----------|--------------|
| Hydrogen-bond interactions |          |                        |          |              |
| Glu550 O <sup>ε1</sup>     | <i>D</i> | Thr209 O <sup>γ</sup>  | <i>H</i> | 2.9          |
| Glu550 O <sup>ε1</sup>     | <i>D</i> | Gln211 N               | <i>H</i> | 3.0          |
| Lys554 N <sup>ε</sup>      | <i>D</i> | Leu359 O               | <i>H</i> | 3.2          |
| van der Waals interactions |          |                        |          |              |
| Glu550 C <sup>β</sup>      | <i>D</i> | Gln211 C <sup>α</sup>  | <i>H</i> | 3.9          |
| Glu550 C <sup>δ</sup>      | <i>D</i> | Gln211 C <sup>β</sup>  | <i>H</i> | 3.8          |
| Glu550 O <sup>ε1</sup>     | <i>D</i> | Gln211 C <sup>α</sup>  | <i>H</i> | 3.6          |
| Glu550 O <sup>ε1</sup>     | <i>D</i> | Gln211 C <sup>β</sup>  | <i>H</i> | 3.5          |
| Lys554 C <sup>ε</sup>      | <i>D</i> | Asp360 C <sup>β</sup>  | <i>H</i> | 4.1          |
| Lys554 N <sup>ε</sup>      | <i>D</i> | Asp360 C <sup>α</sup>  | <i>H</i> | 3.6          |
| Val555 C                   | <i>D</i> | Gln211 C <sup>δ</sup>  | <i>H</i> | 4.1          |
| His556 C <sup>α</sup>      | <i>D</i> | Gln211 C <sup>δ</sup>  | <i>H</i> | 4.0          |
| His556 C <sup>β</sup>      | <i>D</i> | Gln211 C <sup>δ</sup>  | <i>H</i> | 3.7          |
| His556 C <sup>β</sup>      | <i>D</i> | Gln211 O <sup>ε1</sup> | <i>H</i> | 3.4          |
| His556 C <sup>β</sup>      | <i>D</i> | Gln211 N <sup>ε2</sup> | <i>H</i> | 3.7          |

(Krissinel & Henrick, 2007) suggests a tetramer and not an octamer as the most probable multimeric state of the rmGPb–AMP complex structure.

In contrast to the lower resolution T-state rmGPb structure (PDB entry 1gpb; Acharya *et al.*, 1991), in which the coordinates of residues 253–259, 316–323 and 837–841 were reported, in the high-resolution structure these residues were not located within the electron-density map and hence were not modelled. The r.m.s.d. between the two structures (excluding residues 7–18, 253–259, 316–323 and 837–841) is 0.5 and 1.1 Å for main-chain and all atoms, respectively.

Differences between the T-state and R-state rmGPb structures explaining the allosteric activation of the enzyme have been reported in detail previously (Barford & Johnson, 1989; Barford *et al.*, 1991), so we will not discuss them here. However, the high-resolution (1.45 Å) free T-state rmGPb structure reported here led to the identification of residues 7–18 within the electron-density map. The coordinates of these

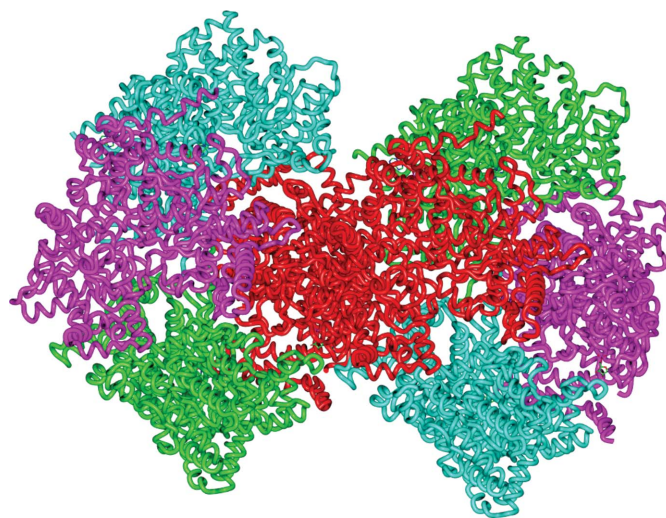


**Figure 1**

Structure of R-state rmGPb–AMP from a crystal grown in the presence of AMP. Structurally equivalent subunits in the two tetramers are shown in the same colour.

residues were not located in the only free T-state GPb structure available thus far (PDB entry 1gpb; Acharya *et al.*, 1991). However, residues 10–18 have been observed in various rmGPb complexes with inhibitors that stabilize the T-state conformation (Stravodimos *et al.*, 2017; Hayes *et al.*, 2014) and their conformation is identical to that in the T-state free structure reported here. The conformation of this N-terminal segment is important since it contains Ser14, phosphorylation of which by glycogen phosphorylase kinase transforms GPb into GPa, activating the enzyme (Barford *et al.*, 1991; Johnson, 1992; Oikonomakos, 2002). Previous comparative structural analysis (Barford & Johnson, 1989) of the free T-state (PDB entry 1gpb) and R-state (PDB entry 9gpb) have revealed that the T-state to R-state transition involves small changes in the tertiary structure at the ligand-binding sites and the subunit-interface regions, and little change in the remainder of the subunit. These are coupled to large changes in quaternary structure that involve rotation of the two subunits with respect to one another. At the serine phosphate site, two arginines (Arg69 and Arg43', where a prime denotes a residue from a neighbouring subunit), one from each of the subunits, move to create the phosphate site, and the presence of the dianion phosphate leads to placement of the basic N-terminal tail opposite the N-terminal helix  $\alpha 1$  (residues 22'–38') and towards the loop connecting helices  $\alpha 4'$  and  $\alpha 5'$  of the neighbouring subunit. Since the N-terminal tail (residues 1–18) was not located in the T-state structure, it was presumed to be disordered and to become ordered upon transition from the T-state to the R-state. However, as revealed from structures of rmGPb–inhibitor complexes at high resolution [for example, PDB entries 2gj4 (Whittamore *et al.*, 2006) and 5lrf (Kantsadi *et al.*, 2017) at 1.6 and 1.75 Å resolution, respectively], residues 12–18 are ordered. In addition, the 1.45 Å resolution structure presented here also revealed the location of residues 7–11 (residues 12–18 have almost the same conformation as in previous T-state rmGPb–inhibitor complexes). Thus, it is now clear that residues 8–17 form an  $\alpha$ -helix (termed now  $\alpha 0$ ) and the side chain of Ser14 forms a hydrogen-bond interaction with the side chain of Glu501, an interaction that is also present in T-state rmGPb–inhibitor complexes. Therefore, the conformation of the N-terminal segment (residues 7–23) is totally different in T-state and R-state rmGPb. The N-terminus points in opposite directions (Fig. 2) and is involved in different interactions. Upon transition from the T-state to the R-state, it performs a significant conformational change that allows it to interact with the neighbouring subunit, further stabilizing the tetramer association. This conformational change is triggered either by the binding of the sulfate anion (Barford & Johnson, 1989) to Ser14 (PDB entry 7gpb) or by the phosphorylation of this serine (PDB entry 1gpa; Barford *et al.*, 1991). This suggestion is further supported by the fact that the N-terminus adopts this conformation not only in the R-state but also in the T-state dimeric rmGPa structure (PDB entry 2gpa; Oikonomakos *et al.*, 1999). The presence of a dianion disrupts the hydrogen-bonding interaction of Ser14 and Glu501 and repulsive forces trigger the conformational change of the N-terminus. As noted

by Barford *et al.* (1991) and Martin *et al.* (1990), this conformational change results in a change in the environment of Ser14 from one that contains clusters of negatively charged groups in the nonphosphorylated state to one that contains clusters of positively charged groups in the phosphorylated state. These conformational changes that create the serine phosphate recognition site also lead to interactions that are important in developing a high-affinity AMP effector site situated 15 Å from the serine phosphate site (Barford *et al.*, 1991).

### 3.2. The binding of AMP and IMP

rmGPb has a much stronger affinity for AMP ( $K_a = 3.1 \mu M$ ) than for IMP ( $K_a = 120 \mu M$ ) in the presence of ammonium sulfate (Leonidas *et al.*, 1990). AMP and IMP bind very similarly at the allosteric site of R-state rmGPb (Fig. 3). The most significant difference lies within the conformation of the AMP loop (residues 313–326). The AMP loop in the rmGPb–AMP complex is well defined within the electron-density map in all rmGPb subunits apart from *C* and *H*. In these rmGPb subunits the AMP loop is involved in crystal-packing contacts and the symmetry subunits impose steric impediments on a conformation such as that it adopts in the other six subunits. In the T-state free rmGPb and the R-state free rmGPb and rmGPb–IMP complex this loop is disordered. In the structure of the R-state PLPP enzyme in complex with AMP (PDB entry 1pyg) the AMP loop adopts a conformation that allows it to form hydrogen bonds from the main-chain carbonyl O atoms of Ala315 and Cys318 to the N6 amino group of AMP, and it was proposed that these interactions favour AMP binding and discriminate against IMP binding at this site (Sprang *et al.*, 1991). In the structure of the R-state rmGPb–AMP complex presented here the AMP loop adopts a very similar conformation and the main-chain carbonyl O atoms of Ala315 and Cys318 are at a hydrogen-bonding distance from N6 of AMP (Table 3). In the structure of the R-state PLPP enzyme in complex with IMP (PDB entry 1abb) the AMP loop is not disordered but adopts a significantly different conformation to that of the native AMP complex presented here, which is too far away to make contacts with the nucleotide



**Figure 2**  
Superimposed structures of R-state (green) and T-state (purple) rmGPb showing the different conformations of the N-terminal segment.

**Table 3**  
AMP–rmGPb interactions in the two crystal forms.

Residues with a prime are from an adjacent subunit.

| AMP atom                                   | rmGPb–AMP (Barford <i>et al.</i> , 1991)   | rmGPb–AMP (co-crystal)  |
|--|--|---|
| Hydrogen-bond interactions (distance in Å) |  |   |
| N1   | Asn44' N <sup>δ2</sup> (3.1)   | Gly317 N (2.8)  |
| N6   |  | Ala315 O (3.4), Cys318 O (3.3)  |
| O2'  |  | Asp42' O <sup>δ2</sup> (2.7)  |
| O1P  | Arg309 N <sup>η2</sup> (2.7)   | Arg309 N <sup>η2</sup> (2.5)  |
| O2P  | Arg309 N <sup>η2</sup> (2.7), Arg310 N <sup>ε</sup> (3.0), N <sup>η2</sup> (2.5)   | Tyr75 O <sup>η</sup> (2.7), Arg310 N <sup>ε</sup> (2.7)   |
| O3P  |  | Arg310 N <sup>η2</sup> (3.2)  |
| van der Waals interactions                 |  |   |
| N1   | Asn44' C <sup>β</sup>  | Gly317 C <sup>α</sup>   |
| N3   | Gln72 C <sup>α</sup> , C <sup>γ</sup>  |   |
| N6   | Tyr75 C <sup>δ2</sup> , C <sup>ε2</sup>  |   |
| N7   | Tyr75 C <sup>γ</sup> , C <sup>δ1</sup> , C <sup>δ2</sup> , C <sup>ε1</sup> , C <sup>ε2</sup> , C <sup>ε</sup>                          | Val45' C <sup>γ2</sup> , Tyr75 C <sup>δ1</sup> , C <sup>ε1</sup> , C <sup>ε2</sup> , C <sup>ε</sup>                                   |
| N9   | Tyr75 C <sup>δ1</sup>  | Tyr75 C <sup>δ1</sup> , C <sup>ε1</sup>   |
| C2   | Asn44' C <sup>β</sup> , C <sup>γ</sup> , N <sup>δ2</sup> , Gln72 C <sup>α</sup> , Glu76 O <sup>ε2</sup>                                | Asn44' C <sup>β</sup> , C <sup>γ</sup> , O <sup>δ1</sup> , Tyr75 C <sup>β</sup> , Phe316 C <sup>δ1</sup> , C <sup>ε1</sup> , Gly317 N |
| C4   | Tyr75 C <sup>γ</sup> , C <sup>δ1</sup> , C <sup>δ2</sup>   | Tyr75 C <sup>γ</sup> , C <sup>δ1</sup> , C <sup>ε1</sup>  |
| C5   | Tyr75 C <sup>β</sup> , C <sup>γ</sup> , C <sup>δ1</sup> , C <sup>δ2</sup> , C <sup>ε1</sup> , C <sup>ε2</sup> , C <sup>ε</sup>         | Tyr75 C <sup>γ</sup> , C <sup>δ1</sup> , C <sup>δ2</sup> , C <sup>ε1</sup> , C <sup>ε2</sup> , C <sup>ε</sup>                         |
| C6   | Asn44' C <sup>β</sup> , Tyr75 C <sup>β</sup> , C <sup>γ</sup> , C <sup>δ2</sup> , C <sup>ε2</sup>                                      | Tyr75 C <sup>β</sup> , C <sup>γ</sup> , C <sup>δ2</sup> , Gly317 N  |
| C8   | Val45' C <sup>γ2</sup> , Tyr75 C <sup>γ</sup> , C <sup>δ1</sup> , C <sup>δ2</sup> , C <sup>ε1</sup> , C <sup>ε2</sup> , C <sup>ε</sup> | Val45' C <sup>γ2</sup> , Tyr75 C <sup>δ1</sup> , C <sup>ε1</sup> , C <sup>ε</sup>   |
| C1'  | Gln71 C, C <sup>β</sup>  | Gln71 C <sup>β</sup> , Tyr75 C <sup>δ1</sup> , C <sup>ε1</sup>  |
| C2'  | Asp42' O <sup>δ2</sup>   | Asp42' C <sup>γ</sup> , O <sup>δ1</sup> , O <sup>δ2</sup>   |
| C3'  | Val45' C <sup>γ1</sup>   |   |
| C4'  | Trp67 C <sup>η2</sup> , Gln71 C <sup>β</sup> , C <sup>γ</sup>  | Trp67 C <sup>η2</sup> , Gln71 C <sup>β</sup> , C <sup>γ</sup>   |
| C5'  | Trp67 C <sup>η2</sup>  | Trp67 C <sup>η2</sup>   |
| O2'  |  | Asp42' C <sup>γ</sup>   |
| O3'  | Asp722' C, O   | Trp67 C <sup>ε3</sup>   |
| O4'  | Gln71 C <sup>β</sup>   | Gln71 C <sup>β</sup> , Tyr75 C <sup>ε1</sup>  |
| P'   | Arg309 N <sup>η2</sup> , Arg310 N <sup>η2</sup>  | Arg309 N <sup>η2</sup>  |
| O1P  | Gln723' C <sup>α</sup> , C <sup>β</sup> , C <sup>γ</sup>   |   |
| O2P  | Arg310 C <sup>ε</sup>  | Tyr75 C <sup>ε1</sup> , C <sup>ε</sup> , Arg310 C <sup>ε</sup>  |
| <b>Total</b>                               | <b>56</b>  | <b>51</b>   |

(Leonidas, Oikonomakos, Papageorgiou, Acharya *et al.*, 1992). Considering that this loop is disordered in all other rmGPb–IMP complex structures (R-state or T-state), this may offer a structural explanation for the significant differences in the binding affinities of rmGPb for IMP and AMP.

Since we report here the structure of the R-state rmGPb–AMP complex from a crystal grown in the presence of the physiological activator AMP, it will be of interest to compare it with the R-state rmGPb–AMP complex structure determined from preformed R-state rmGPb crystals soaked in AMP solution (Barford *et al.*, 1991; PDB entry 7gpb). This comparison reveals some significant details of AMP binding

and the conformational changes that accompany it. The r.m.s.d. between the structures of the rmGPb–AMP co-crystals and the rmGPb–AMP complex from a soaking experiment (PDB entry 7gpb; Barford *et al.*, 1991), excluding residues 7–10, 251–261 and 281–287, for all atoms of each of the two tetramers of the rmGPb–AMP complex is 1.5 and 1.6 Å, respectively. Of interest, the loop composed of residues 251–261 was not located within the electron-density map of the rmGPb–AMP complex from co-crystallization experiments, while in PDB entry 7gpb its structure is reported. Although the two AMP molecules seem to bind similarly, there are some significant differences in their interactions with the rmGPb

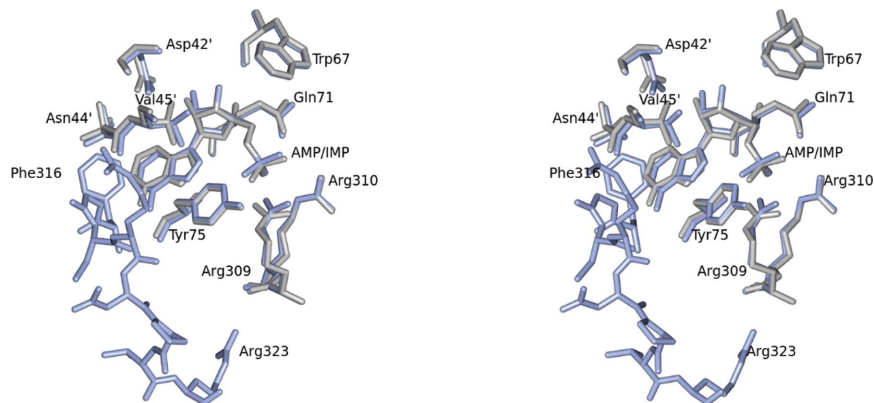


**Figure 3**  
A stereoview of the superimposed structures of R-state rmGPb–AMP (cyan) and R-state rmGPb–IMP complex (grey) at the allosteric binding site.

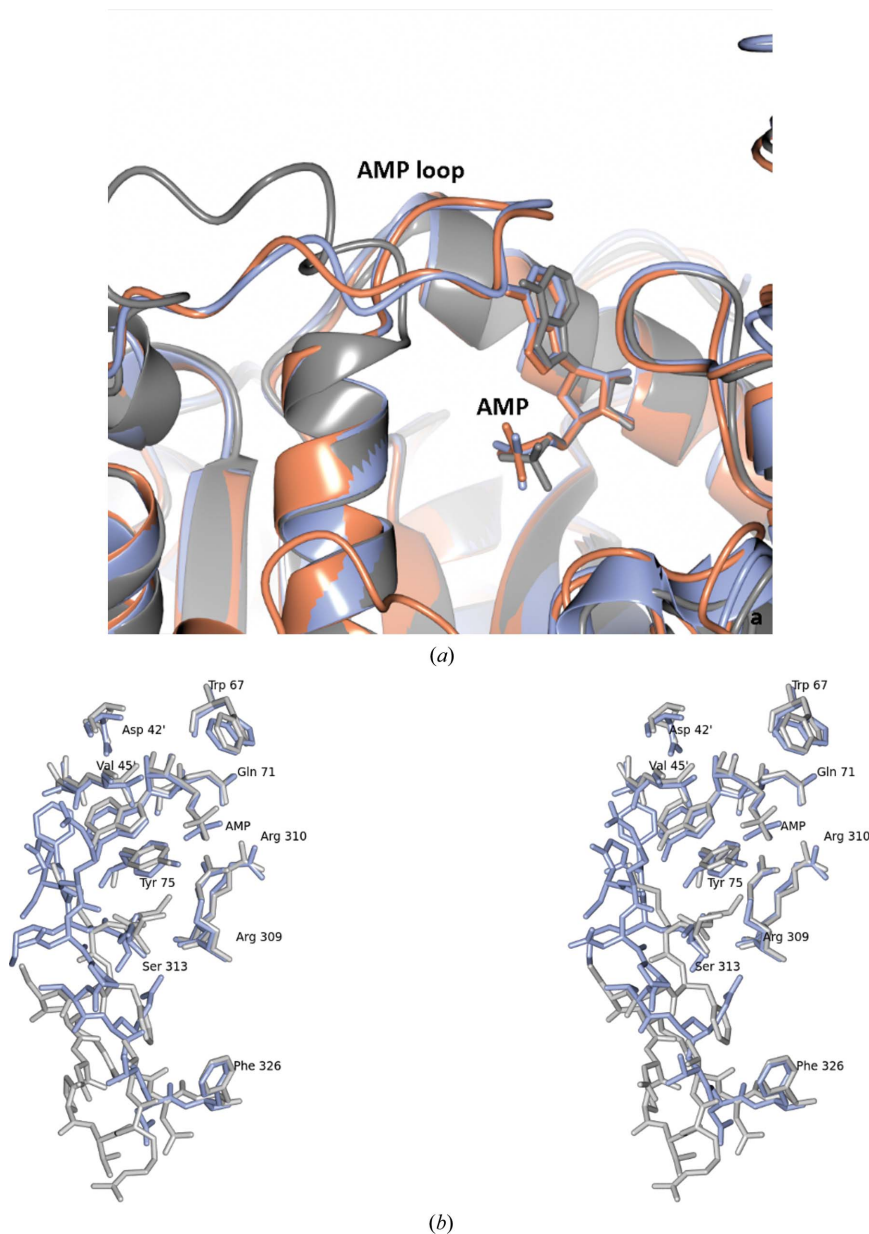


**Figure 4**

Superimposed structures of R-state rmGPb–AMP from co-crystallization (cyan), the structure from a soaking experiment (grey; PDB entry 7gpb) and that of the R-state PLPP enzyme (orange) at the allosteric binding site. Overall structures showing the AMP loop (*a*) and the residues interacting with AMP in stereo (*b*).

residues (Fig. 4). In the rmGPb–AMP complex structure (PDB entry 7gpb; Barford *et al.*, 1991), AMP forms five hydrogen bonds to Arg309, Arg310 and Asn44' from the neighbouring subunit. In the rmGPb–AMP complex from a co-crystallization experiment, AMP also participates in five hydrogen-bond interactions, but with Tyr75, Arg309, Arg310, Gly317 and Asp42' from the neighbouring subunit (Table 3). The number of van der Waals interactions is similar in the two complexes: 56 and 51 for the structures from soaking and co-crystallization experiments, respectively. The most significant structural difference between the two structures in the AMP-binding site is found in the conformation of the AMP loop (r.m.s.d. of 7.2 Å; Fig. 4). The conformation of the AMP loop

(residues 313–326) observed in the complex from the co-crystallization experiment leads to a more extensive burial of AMP in the GPb allosteric site than in PDB entry 7gpb. This becomes more evident from the increase in the solvent area that is made inaccessible upon the binding of AMP in the two complexes. Some 75% of the solvent-accessible area (356 Å<sup>2</sup>) is buried following binding of AMP to the rmGPb–AMP co-crystallized form, compared with 70% (334 Å<sup>2</sup>) of the solvent-accessible area that is buried on binding to the complex in PDB entry 7gpb (Barford *et al.*, 1991).

There is no obvious explanation as to why the binding of AMP triggers two different conformations of the AMP loop in the two structures of rmGPb [one from a soaking experiment

(Barford *et al.*, 1991; PDB entry 7gpb) and the other from co-crystallization]. In both structures the AMP loop is involved in crystal-packing contacts with residues 523–529 of subunit C. However, we could assume that the AMP loop conformation is more physiologically relevant in the structure derived from crystals grown from the rmGPb–AMP complex formed in solution. In support of this assumption, superposition of the two complex structures reveals that the AMP loop conformation in the structure derived from co-crystallization experiments could be adopted in the crystal form of the rmGPb–AMP complex from soaking experiments but would not form any packing contacts. Furthermore, the AMP loop in the structure from co-crystallization adopts a conformation that is very similar to that of the R-state PLPP enzyme in complex with AMP (PDB entry 1pyg; Fig. 4*a*), which was determined from a crystal with a different space group ( $P2_12_12$ ) and different unit-cell dimensions (Sprang *et al.*, 1991). This suggests that this loop, which is disordered in the free structure, becomes ordered upon AMP or IMP binding and adopts a conformation that is mainly dictated by the type of nucleotide that binds at this site.

### Acknowledgements

Work at the Synchrotron Radiation Source, MAX-lab, Lund, Sweden and EMBL Hamburg Outstation, Germany was supported by the European Community's Seventh Framework Programme (FP7/2007-2013) under BioStruct-X (grant agreement No. 283570).

### References

Acharya, K. R., Stuart, D. I., Varvill, K. M. & Johnson, L. N. (1991). *Glycogen Phosphorylase B: Description of the Protein Structure*. Singapore/London: World Scientific.

Agius, L. (2015). *Mol. Aspects Med.* **46**, 34–45.

Barford, D., Hu, S.-H. & Johnson, L. N. (1991). *J. Mol. Biol.* **218**, 233–260.

Barford, D. & Johnson, L. N. (1989). *Nature*, **340**, 609–616.

Barford, D. & Johnson, L. N. (1992). *Protein Sci.* **1**, 472–493.

Bokor, E., Kyriakis, E., Solovou, T. G. A., Koppány, C., Kantsadi, A. L., Szabó, K. E., Szakács, A., Stravodimos, G. A., Docsa, T., Skamnaki, V. T., Zographos, S. E., Gergely, P., Leonidas, D. D. & Somsák, L. (2017). *J. Med. Chem.* **60**, 9251–9262.

Brünger, A. T., Adams, P. D., Clore, G. M., DeLano, W. L., Gros, P., Grosse-Kunstleve, R. W., Jiang, J.-S., Kuszewski, J., Nilges, M., Pannu, N. S., Read, R. J., Rice, L. M., Simonson, T. & Warren, G. L. (1998). *Acta Cryst.* **D54**, 905–921.

Chetter, B. A., Kyriakis, E., Barr, D., Karra, A. G., Katsidou, E., Koulas, S. M., Skamnaki, V. T., Snape, T. J., Psarra, A. G., Leonidas, D. D. & Hayes, J. M. (2020). *Bioorg. Chem.* **102**, 104003.

Chrysina, E. D., Kosmopoulou, M. N., Tiraidis, C., Kardakaris, R., Bischler, N., Leonidas, D. D., Hadady, Z., Somsák, L., Docsa, T., Gergely, P. & Oikonomakos, N. G. (2005). *Protein Sci.* **14**, 873–888.

Cori, C. F., Schmidt, G. & Cori, G. T. (1939). *Science*, **89**, 464–465.

Cori, G. T. & Cori, C. F. (1940). *J. Biol. Chem.* **135**, 733–756.

Cori, G. T. & Green, A. A. (1943). *J. Biol. Chem.* **151**, 31–38.

Drakou, C. E., Gardeli, C., Tsiartas, I., Alexopoulos, S., Mallouchos, A., Koulas, S. M., Tsagkarakou, A. S., Asimakopoulos, D., Leonidas, D. D., Psarra, A. G. & Skamnaki, V. T. (2020). *J. Agric. Food Chem.* **68**, 10191–10199.

Emsley, P., Lohkamp, B., Scott, W. G. & Cowtan, K. (2010). *Acta Cryst.* **D66**, 486–501.

Evans, P. R. & Murshudov, G. N. (2013). *Acta Cryst.* **D69**, 1204–1214.

Fischer, T., Koulas, S. M., Tsagkarakou, A. S., Kyriakis, E., Stravodimos, G. A., Skamnaki, V. T., Liggri, P. G. V., Zographos, S. E., Riedl, R. & Leonidas, D. D. (2019). *Molecules*, **24**, 1322.

French, S. & Wilson, K. (1978). *Acta Cryst.* **A34**, 517–525.

Green, A. A. & Cori, G. T. (1943). *J. Biol. Chem.* **151**, 21–29.

Hayes, J. M., Kantsadi, A. L. & Leonidas, D. D. (2014). *Phytochem. Rev.* **13**, 471–498.

Johnson, L. N. (1992). *FASEB J.* **6**, 2274–2282.

Johnson, L. N. & Barford, D. (1990). *J. Biol. Chem.* **265**, 2409–2412.

Kabsch, W. (2010). *Acta Cryst.* **D66**, 125–132.

Kantsadi, A. L., Apostolou, A., Theofanous, S., Stravodimos, G. A., Kyriakis, E., Gorgogietas, V. A., Chatzileontiadou, D. S., Pegiou, K., Skamnaki, V. T., Stagos, D., Kouretas, D., Psarra, A. M., Haroutounian, S. A. & Leonidas, D. D. (2014). *Food Chem. Toxicol.* **67**, 35–43.

Kantsadi, A. L., Bokor, E., Kun, S., Stravodimos, G. A., Chatzileontiadou, D. S., Leonidas, D. D., Juhász-Tóth, E., Szakács, A., Batta, G., Docsa, T., Gergely, P. & Somsák, L. (2016). *Eur. J. Med. Chem.* **123**, 737–745.

Kantsadi, A. L., Stravodimos, G. A., Kyriakis, E., Chatzileontiadou, D. S. M., Solovou, T. G. A., Kun, S., Bokor, E., Somsák, L. & Leonidas, D. D. (2017). *J. Struct. Biol.* **199**, 57–67.

Krissinel, E. & Henrick, K. (2007). *J. Mol. Biol.* **372**, 774–797.

Kun, S., Begum, J., Kyriakis, E., Stamat, E. C. V., Barkas, T. A., Szennyes, E., Bokor, E., Szabó, K. E., Stravodimos, G. A., Sipos, A., Docsa, T., Gergely, P., Moffatt, C., Patraskaki, M. S., Kokolaki, M. C., Gkerdi, A., Skamnaki, V. T., Leonidas, D. D., Somsák, L. & Hayes, J. M. (2018). *Eur. J. Med. Chem.* **147**, 266–278.

Kyriakis, E., Karra, A. G., Papaioannou, O., Solovou, T., Skamnaki, V. T., Liggri, P. G. V., Zographos, S. E., Szennyes, E., Bokor, E., Kun, S., Psarra, A. G., Somsák, L. & Leonidas, D. D. (2020). *Bioorg. Med. Chem.* **28**, 115196.

Kyriakis, E., Solovou, T. G. A., Kun, S., Czifrák, K., Szócs, B., Juhász, L., Bokor, E., Stravodimos, G. A., Kantsadi, A. L., Chatzileontiadou, D. S. M., Skamnaki, V. T., Somsák, L. & Leonidas, D. D. (2018). *Bioorg. Chem.* **77**, 485–493.

Laskowski, R. A., MacArthur, M. W., Moss, D. S. & Thornton, J. M. (1993). *J. Appl. Cryst.* **26**, 283–291.

Leonidas, D. D., Oikonomakos, N. G. & Papageorgiou, A. C. (1991). *Biochim. Biophys. Acta*, **1076**, 305–307.

Leonidas, D. D., Oikonomakos, N. G., Papageorgiou, A. C., Acharya, K. R., Barford, D. & Johnson, L. N. (1992). *Protein Sci.* **1**, 1112–1122.

Leonidas, D. D., Oikonomakos, N. G., Papageorgiou, A. C. & Sotiroidis, T. G. (1992). *Protein Sci.* **1**, 1123–1132.

Leonidas, D. D., Oikonomakos, N. G., Papageorgiou, A. C., Xenakis, A., Cazianis, C. T. & Bem, F. (1990). *FEBS Lett.* **261**, 23–27.

Lorek, A., Wilson, K. S., Sansom, M. S., Stuart, D. I., Stura, E. A., Jenkins, J. A., Zanotti, G., Hajdu, J. & Johnson, L. N. (1984). *Biochem. J.* **218**, 45–60.

Lukacs, C. M., Oikonomakos, N. G., Crowther, R. L., Hong, L.-N., Kammlott, R. U., Levin, W., Li, S., Liu, C.-M., Lucas-McGady, D., Pietranico, S. & Reik, L. (2006). *Proteins*, **63**, 1123–1126.

Martin, J. L., Johnson, L. N. & Withers, S. G. (1990). *Biochemistry*, **29**, 10745–10757.

Mathieu, C., Li de la Sierra-Gallay, I., Duval, R., Xu, X., Coccagn, A., Léger, T., Woffendin, G., Camadro, J.-M., Etchebest, C., Haouz, A., Dupret, J.-M. & Rodrigues-Lima, F. (2016). *J. Biol. Chem.* **291**, 18072–18083.

Matthews, B. W. (1968). *J. Mol. Biol.* **33**, 491–497.

McNicholas, S., Potterton, E., Wilson, K. S. & Noble, M. E. M. (2011). *Acta Cryst.* **D67**, 386–394.

Monod, J., Wyman, J. & Changeux, J.-P. (1965). *J. Mol. Biol.* **12**, 88–118.

Murshudov, G. N., Skubák, P., Lebedev, A. A., Pannu, N. S., Steiner, R. A., Nicholls, R. A., Winn, M. D., Long, F. & Vagin, A. A. (2011). *Acta Cryst.* **D67**, 355–367.

- Oikonomakos, N. G. (2002). *Curr. Protein Pept. Sci.* **3**, 561–586.
- Oikonomakos, N. G. & Somsák, L. (2008). *Curr. Opin. Investig. Drugs*, **9**, 379–395.
- Oikonomakos, N. G., Tsitsanou, K. E., Zographos, S. E., Skamnaki, V. T., Goldmann, S. & Bischoff, H. (1999). *Protein Sci.* **8**, 1930–1945.
- Otwinowski, Z. & Minor, W. (1997). *Methods Enzymol.* **276**, 307–326.
- Painter, J. & Merritt, E. A. (2006). *J. Appl. Cryst.* **39**, 109–111.
- Rath, V. L., Ammirati, M., LeMotte, P. K., Fennell, K. F., Mansour, M. N., Danley, D. E., Hynes, T. R., Schulte, G. K., Wasilko, D. J. & Pandit, J. (2000). *Mol. Cell*, **6**, 139–148.
- Somsák, L. (2011). *C. R. Chim.* **14**, 211–223.
- Somsák, L., Czifrák, K., Tóth, M., Bokor, E., Chrysina, E. D., Alexacou, K. M., Hayes, J. M., Tiraidis, C., Lazoura, E., Leonidas, D. D., Zographos, S. E. & Oikonomakos, N. G. (2008). *Curr. Med. Chem.* **15**, 2933–2983.
- Sprang, S. & Fletterick, R. J. (1979). *J. Mol. Biol.* **131**, 523–551.
- Sprang, S. R., Withers, S. G., Goldsmith, E. J., Fletterick, R. J. & Madsen, N. B. (1991). *Science*, **254**, 1367–1371.
- Stravodimos, G. A., Chetter, B. A., Kyriakis, E., Kantsadi, A. L., Chatzileontiadou, D. S., Skamnaki, V. T., Kato, A., Hayes, J. M. & Leonidas, D. D. (2017). *Curr. Med. Chem.* **24**, 384–403.
- Storoni, L. C., McCoy, A. J. & Read, R. J. (2004). *Acta Cryst.* **D60**, 432–438.
- Treadway, J. L., Mendys, P. & Hoover, D. J. (2001). *Expert Opin. Investig. Drugs*, **10**, 439–454.
- Whittamore, P. R., Addie, M. S., Bennett, S. N., Birch, A. M., Butters, M., Godfrey, L., Kenny, P. W., Morley, A. D., Murray, P. M., Oikonomakos, N. G., Otterbein, L. R., Pannifer, A. D., Parker, J. S., Readman, K., Siedlecki, P. S., Schofield, P., Stocker, A., Taylor, M. J., Townsend, L. A., Whalley, D. P. & Whitehouse, J. (2006). *Bioorg. Med. Chem. Lett.* **16**, 5567–5571.
- Winn, M. D., Ballard, C. C., Cowtan, K. D., Dodson, E. J., Emsley, P., Evans, P. R., Keegan, R. M., Krissinel, E. B., Leslie, A. G. W., McCoy, A., McNicholas, S. J., Murshudov, G. N., Pannu, N. S., Potterton, E. A., Powell, H. R., Read, R. J., Vagin, A. & Wilson, K. S. (2011). *Acta Cryst.* **D67**, 235–242.